JACS
JOURNAL OF THE AMERICAN CHEMICAL SOCIETY

Article

pubs.acs.org/JACS

Dendron-Mediated Engineering of Interparticle Separation and Self-Assembly in Dendronized Gold Nanoparticles Superlattices

Davit Jishkariani,[†,‡] Benjamin T. Diroll,[†] Matteo Cargnello,[†,⊥] Dahlia R. Klein,[†] Lawrence A. Hough,[‡] Christopher B. Murray,*[,†,∥] and Bertrand Donnio*[,‡,§]

[†]Department of Chemistry, University of Pennsylvania, Philadelphia, Pennsylvania 19104, United States

[‡]Complex Assemblies of Soft Matter Laboratory (COMPASS), UMI 3254, CNRS-Solvay-University of Pennsylvania, CRTB, 350 George Patterson Boulevard, Bristol, Pennsylvania 19007, United States

[§]Institut de Physique et Chimie des Matériaux de Strasbourg (IPCMS), UMR 7504, CNRS-Université de Strasbourg, 23 rue du Loess, BP43, Strasbourg 67034 Cedex 2, France

[∥]Department of Materials Science and Engineering, University of Pennsylvania, Philadelphia, Pennsylvania 19104, United States

Supporting Information

ABSTRACT: Self-assembly of nanoparticles into designed structures with controlled interparticle separations is of crucial importance for the engineering of new materials with tunable functions and for the subsequent bottom-up fabrication of functional devices. In this study, a series of lipophilic, highly flexible, disulfide dendritic wedges (generations 0−4), based on 2,2-bis(hydroxymethyl)propionic acid, was designed to bind Au nanoparticles with a thiolate bond. By controlling the solvent evaporation rate, the corresponding dendron-capped Au hybrids were found to self-organize into hexagonal close-packed (*hcp*) superlattices. The interparticular spacing was progressively varied from 2.2 to 6.3 nm with increasing dendritic generation, covering a range that is intermediate between commercial ligands and DNA-based ligand shells. Dual mixtures made from some of these dendronized hybrids (i.e., same inner core size but different dendritic covering) yielded binary superlattice structures of unprecedented single inorganic components, which are isostructural with $NaZn_{13}$ and $CaCu_5$ crystals.

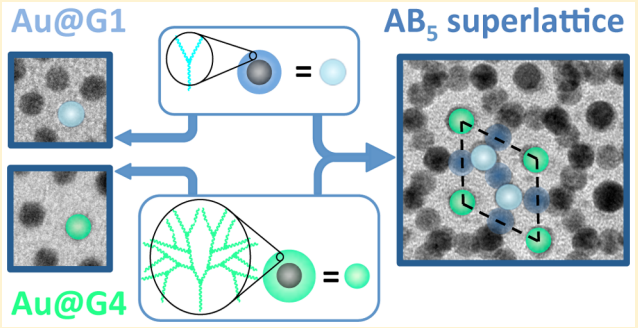

INTRODUCTION

The collective physical properties of nanoparticle (NP) assemblies depend strongly on interparticle distance. The controlled tuning of interparticle spacings offers the possibility to optimize the response of NP solids for applications including optical, magnetic and electronic devices.[1−7] One well-known example of distance-dependent response is the localized surface plasmon resonance of metallic NPs, and particularly of gold and silver NPs.[8−12] Although substantial efforts have been made to decrease interparticular spacings in NP solids,[6] typically for enhanced conductivity, many optical phenomena such as plasmonic enhancement of photoluminescence have ideal interparticle separations greater than the 1−2 nm that is typically accessed with commercially available ligands, such as alkylthiols (including dithiol and disulfide-based ligands), ω-functionalized alkylthiols, etc. To date, lithographic methods have been used to study these effects,[11,13] but recently, new "softer" bottom-up approaches including DNA hybridization of NPs,[14−19] liquid-crystals functionalization,[20−23] liquid crystals defects[20,23,24] and block copolymers surface templates[25] have been reported, and shown to allow precise control over the NPs assemblies (NP separations and symmetries of the arrangements).[9,11,13,26,27] Of relevance to this work, interparticle spacings modulation in the range of 0.6−1.9 nm were achieved in binary mixtures of poly(amidoamine) dendrimers (PAMAM, G0−G4) and mercaptoundecanoic acid passivated gold NPs prepared via co-precipitation, but without control of the ordering.[28] In all cases, the distance modulation is presented in dimers, trimers, or in small particles clusters, and the accessible range has been limited by the size of the organic templates. Replicating this interparticle distance control while still preserving ordered assemblies of NPs over large areas with high uniformity is an important challenge and is inevitable for the fabrication of solid-state devices and metamaterials based on NPs.

Herein, we present our strategy that utilizes soft, lipophilic dendritic ligands as monodisperse and homogeneous organic NP coatings to foster the formation of NP superlattices with a precise control over interparticle distances in a range that is intermediate between commercial and DNA-based ligands. Dendritic molecules are pertinent ligands for NP functionalization in that they possess controlled functionality, monodisperse size, and adaptive generation-dependent morphology (cone

Received: June 17, 2015
Published: August 10, 2015

DOI: 10.1021/jacs.5b06306
J. Am. Chem. Soc. 2015, 137, 10728−10734

Scheme 1. Synthesis of the Diazido Anchoring Unit, 4, Dendritic Alkyne, and Disulfide Wedges G0-4, and Corresponding Dendronized Gold Hybrids Au@G0-4[a]

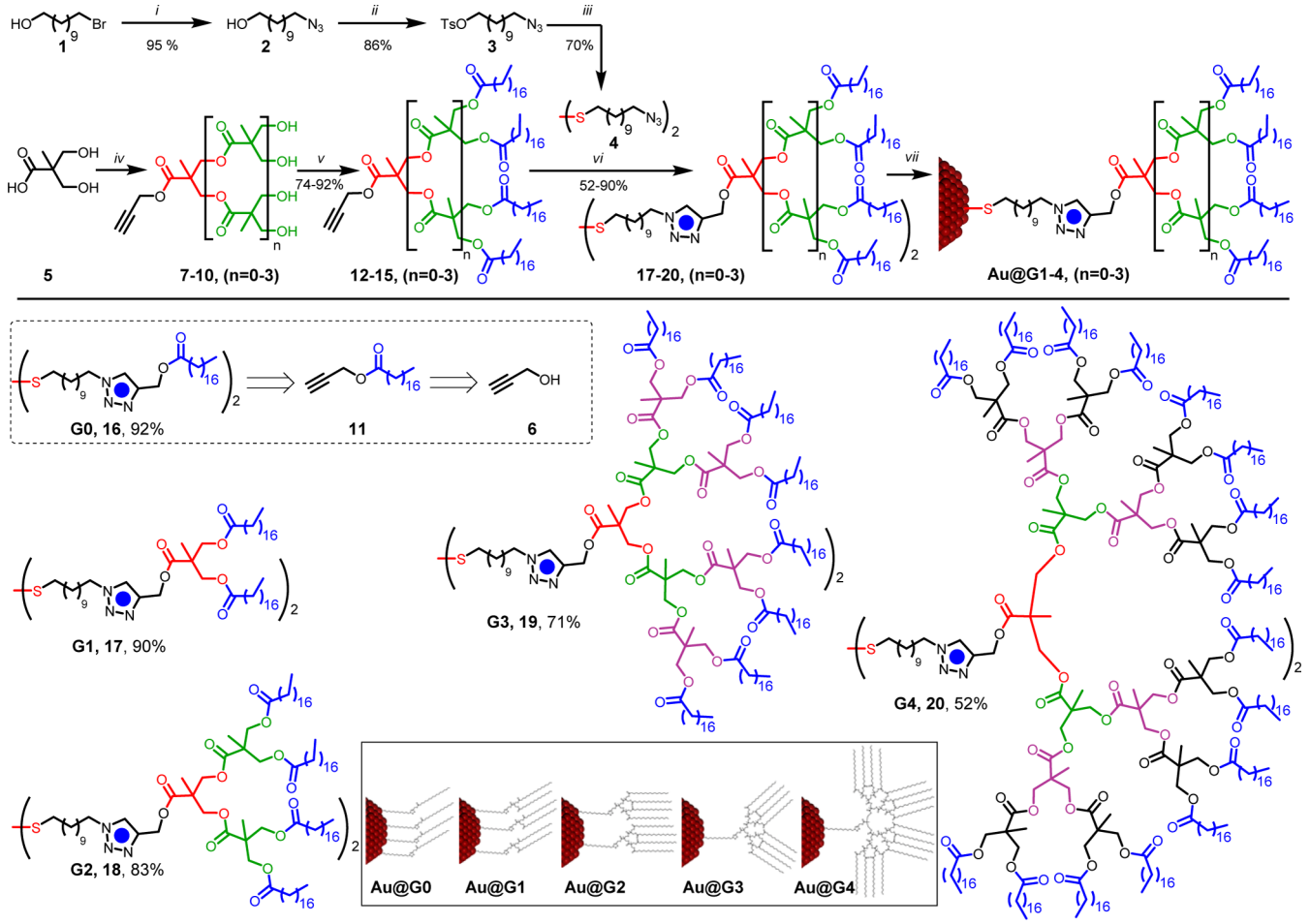

[a]Reagents and conditions: (i) NaN_3, DMF, 70 °C, 12 h; (ii) TsCl, Et_3N, CH_2Cl_2, rt, 12 h; (iii) thiourea, EtOH, 80 °C, 12 h, then I_2, MeOH, rt, 30 min. (iv) See Supporting Information for details; (v) stearic anhydride, DMAP, pyridine, CH_2Cl_2, 12 h; (vi) **4**, $Cu(SO_4)$ $5H_2O$ (20 mol %), sodium ascorbate (40 mol %), THF/H_2O = 4/1, MW, 60 °C, 2–6 h; (vii) oleylamine caped Au@NPs (Au@OLAM), $CHCl_3$, rt, 20 min.

angle variability).[29−32] Due to their high flexibility and deformability, well ordered NP assemblies can still be formed even in systems having larger size/shape distribution discrepancies. Previous reports on nanoparticle-cored dendrimers prepared directly in the presence of dendrimers[33] or via solvent-mediated dendritic ligand exchange reaction[34−37] have included the study of spacing-dependent dipolar interactions in 2D arrays of iron oxide NPs,[38] liquid-crystalline self-assemblies of dendronized gold nanoparticles,[39−41] construction of covalently bound dendrimer−NP multilayers,[42] and the use of dendronized hybrid systems in drug delivery,[43−45] imaging and theranostics,[46] and sensing for selective ion recognition,[47,48] as well as recoverable catalysts.[49]

RESULTS AND DISCUSSION

Disulfide dendritic wedges of generations 1−4, based on 2,2-bis(hydroxymethyl)propionic acid scaffold (bis-MPA, **5**, Scheme 1) were synthesized by the Cu(I)-catalyzed cycloaddition "click" reaction between the azide-terminated anchoring unit **4** and the alkynic branches **12**−**15** (Scheme 1). The anchoring unit **4** was prepared in a three-step, high-yield synthesis from commercially available 11-bromoundecanol **1** (Scheme 1) and derivatized with a disulfide function to bind effectively to Au NPs.[50]

The synthesis of the branched polyester scaffolds **7**−**10** was achieved via divergent iterative anhydride coupling according to reported methods.[51−54] The hydroxyl end groups of the dendrons were then selectively reacted with stearic anhydride to provide desired steric and solubility properties (**12**−**15**, Scheme 1). In addition, the nonbranched system, G0, was prepared for comparison by direct esterification of stearic anhydride with propargyl alcohol (**11**, inset Scheme 1). The disulfide compounds synthesized as described above were used to perform ligand exchange on 5.8 nm-diameter Au NPs capped with oleylamine (Au@OLAM, Figure S1). The mechanism of disulfide addition is presumed to be similar to self-assembled monolayers.[55] After ligand exchange, which was performed by stirring Au@OLAM in a chloroform solution containing the displacing dendritic ligand, unbound organic material was removed by repeated precipitation with antisolvent (2-propanol/ethanol mixtures) and centrifugation. The resulting dendronized hybrids Au@Gn (n = 0−4) could be redispersed in chloroform, toluene, hexanes, or other nonpolar solvents. As a standard against which the dendritic effect can be evaluated, ligand exchange was also performed with 1-

DOI: 10.1021/jacs.5b06306
J. Am. Chem. Soc. 2015, 137, 10728−10734

dodecanethiol (DDT), which is a common ligand for gold NPs (Au@DDT).

The detailed syntheses of the dendritic ligands and characterization data are provided in the Supporting Information. The presence of the dendritic coating on the NP surface and the effect on interparticle spacing were confirmed by a combination of techniques including FTIR, NMR, and UV−vis spectroscopies; thermogravimetric analysis (TGA); transmission electron microscopy (TEM); and small-angle X-ray scattering (SAXS). Unambiguous results were obtained when solution phase NMR spectroscopy was used.

^{1}H NMR spectroscopy demonstrating ligand exchange is shown in Figure 1. In addition to aliphatic protons, several

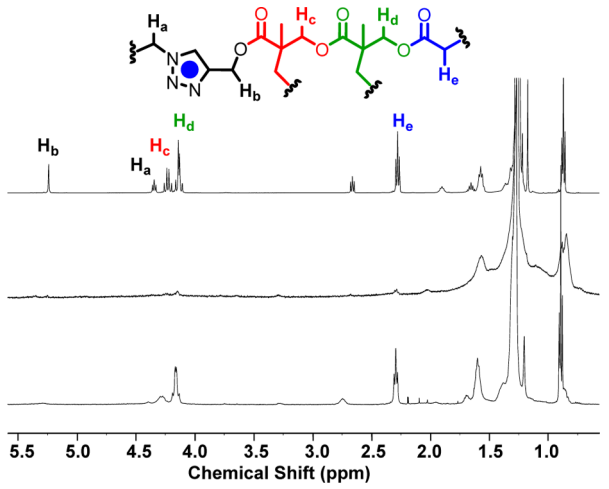

Figure 1. ^{1}H NMR spectra ($CDCl_3$, 500 MHz) of free disulfide G2 (top), Au@G2 (middle), and disulfide G2 dendron after iodine treatment of Au@G2 (bottom).

spectral resonances of the free dendritic ligand (G2 in this case) can be assigned as shown. Once ligand exchange has proceeded, a substantial broadening of the representative proton signals of the dendrons was observed (Figure 1), to such an extent that some resonances were no longer distinguishable from the baseline. This phenomenon essentially accounts to the hindered and slower dynamics of the dendrons bound to the NP with respect to those of the free ligands, the time scale of the NMR presenting an average of all possible conformations.[56]

Furthermore, when the sample in solution was treated with iodine, the thiol-containing dendritic ligands were oxidized off of the Au NP surface (Figure 1), as NMR shows that the specific signals from the ligand are mostly recovered after iodine oxidation. Albeit destructive, this method provides an unambiguous proof of the presence of dendritic ligands on Au NP surfaces. The absence of residual OLAM on the NP surface was also identified by FTIR, which revealed the disappearance of the peak at ca. 3000 cm^{-1} of the amine (Figure S2).

The grafting density on the gold surface was determined from TGA measurements (Figure S3). The organic weight fraction for each sample was obtained by heating under air to 500 °C. These measurements showed that essentially all the oleylamine ligands were displaced by the disulfide-containing ligands, which form a stronger bond with gold. A substantial enhancement of the overall thermal stability of the dendronized hybrids with respect to the OLAM-precursor and the DDT-capped Au NP (from ca. 50 up to 100 °C) was also observed upon increasing the dendritic generation, which suggests that the numerous diverging liphophilic chains are tightly packed in the shell corona and efficiently shield the inorganic core.[33] The volume fractions of the organic parts, directly deduced from the weight fractions and reasonably assuming a density of 0.9 g·cm^{-3} for the dendrons (due to their lipophilic nature and low-temperature solid behavior, Figure S4), allowed estimations of the number of ligands per Au NP, hybrids' radii, and grafting densities. The Au@DDT and Au@OLAM samples showed similar grafting densities, which, as expected, decreased with each new generation, most likely due to steric hindrance (Table 1). Corollary, the hybrids' diameters also increase steadily with the size of the dendrons (Figure S5).

To provide a visual demonstration of the ligand-mediated interparticle spacings, NP monolayer assemblies were obtained by drop-casting dilute hexanes dispersions of the hybrids (<1 mg mL^{-1}) onto diethylene glycol liquid surfaces, followed by controlled evaporation.[5] TEM micrographs (Figure 2) show the progressive increase of interparticle separation from Au@DDT to Au@G4.

SAXS of the Au hybrid solids, shown in Figure 3a, confirm that the increase in interparticle spacing apparent from the TEM images is replicated throughout drop-cast NP solid films (Table 1). The maximum of the first peak of the samples shift systematically from a value of q = 0.825 nm^{-1} for Au@DDT to q = 0.545 nm^{-1} for Au@G4, indicative of an overall increase in

Table 1. Plasmonic and Structural Properties of the Dendronized Hybrids[a]

L (Au@L)	λ_{max}/nm	q/nm^{-1}	d/nm	a/nm	s/nm	MW/g mol^{-1}	wt %	n_L	f	ϕ_{hyb}/nm	s'/nm	δ/L nm^{-2}	σ/Å^2
DDT	575	0.825	7.6	8.0	2.2	202.4	7.4	469	64.5	8.2	2.4	4.5	22.2
G0	554	0.715	8.8	9.2	3.4	551.9	14.7	371	78.7	9.7	3.9	3.5	28.6
G1	535	0.685	9.2	9.6	3.8	934.5	16.9	259	81.3	10.2	4.4	2.5	40.0
G2	534	0.605	10.4	10.9	5.1	1699.7	20.0	175	84.3	10.8	5.0	1.6	60.6
G3	531	0.595	10.6	11.1	5.3	3230.0	21.0	98	85.1	11.0	5.1	0.9	111.1
G4	528	0.545	11.5	12.1	6.3	6290.7	28.0	73	89.3	12.2	6.4	0.7	142.8
OLAM	-	-	-	-	-	267.5	9.0	440	70.2	8.6	2.9	4.2	23.8

[a]L: ligand type on the NP surface (G0−G4 are thiol-containing dendrons). λ_{max}: maximum of the absorption wavelength in solid films. q: q-vector; $d = 2\pi/q$, diffraction spacing; $a = [3d \text{ Log } 3]/\pi$,[57] average interparticular distance; $s = a - \phi$, edge-to-edge separation, from SAXS (ϕ = 5.8 nm, NP diameter). MW: ligand molecular weight. wt %: weight fraction of ligands, from TGA; $n_L = \{\text{wt \%(L)}/[1 - \text{wt \%(L)}]\}$. $[MW_{Au@NP}/MW_L]$, number of (thiol) ligands grafted on the NP surface; $MW_{Au@NP} = n_{Au} \cdot MW_{Au} = 1.19 \times 10^6$ g mol^{-1}, molecular weight of NP; MW_{Au} = 196.967 g mol^{-1}; $V_{Au@NP} = 4\pi(\phi/2)^3/3$ = 102.2 nm^3, NP volume; V_{Au} = 16.923 Å^3; $n_{Au} = V_{Au@NP}/V_{Au}$ = 6036−6037, number of Au atoms in NP; $f = n_L V_L/(n_L V_L + V_{Au@NP})$, ligand volume fraction; $V_L = n_L[MW_L/0.6022\rho]$, volume of the dendritic part estimated assuming a density, ρ = 0.9 g cm^{-3} (for DDT and OLAM, ρ = 0.85 and 0.813 g cm^{-3}, respectively); $\phi_{hyb} = \phi/[(1 - f)]^{1/3}$, hybrid diameter; $s' = \phi_{hyb} - \phi$, edge-to-edge separation, from TGA; $\delta = n_L/4\pi(\phi/2)^2$, grafting density; $\sigma = 100/\delta$, ligand cross-section area.

DOI: 10.1021/jacs.5b06306
J. Am. Chem. Soc. 2015, 137, 10728−10734

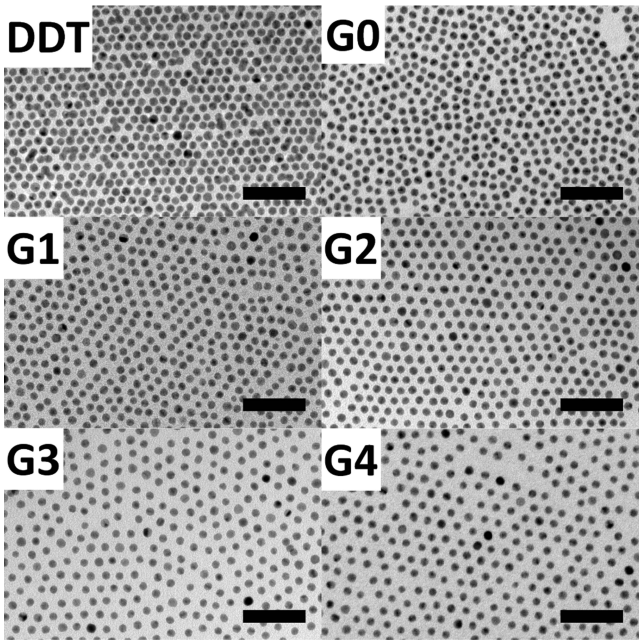

Figure 2. TEM micrographs of monolayers of Au@DDT and Au@G0-G4. Scale bars are 50 nm.

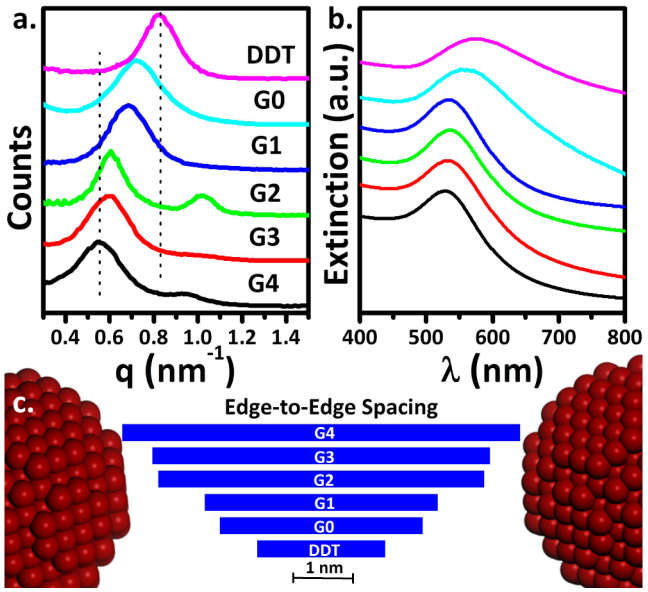

Figure 3. (a) Transmission SAXS of thin solid films composed of Au@L (L = DDT, G0-G4). (b) Extinction spectra of thin solid films composed of Au@L, normalized to the absorption maximum and offset for clarity. Same color code for both figures. (c) Schematic representation of the average interparticle edge-to-edge spacings of solids composed of Au@L hybrids deduced from SAXS.

separation of approximately 4 nm. Although all the samples are glasses as evidenced by the broadness of the fundamental small-angle reflection (Figure 3a), they nevertheless all exhibit short-range hexatic ordering as revealed by TEM images (Figure 2).

Au@G2 and Au@G4 in particular show an additional diffuse reflection, with the center electron density maximum in spacing ratio $\sqrt{3}$ with respect to first diffraction signal: these two reflections coincide with the first reflections of a hexagonal lattice. We estimate based upon particle sizing measurements that this corresponds to an edge-to-edge spacing of 2.2 nm for Au@DDT increasing to 6.3 nm for Au@G4, assuming an average hexagonal environment for all the samples (s, Table 1).[57] The interparticle distances calculated from TGA data are in very close agreement to the results obtained from X-ray diffraction (comparison of a and $\phi_{hyb,}$, the hybrid diameter, or s and s', Table 1, Figure S5). This suggests that the soft ligands, and particularly those of smaller generation, deform from a spherical shell to distorted polyhedron in order to more efficiently fill interstices in the solid state.

The dramatic change in interparticle spacing is also apparent in the extinction spectra shown in Figure 3b. In the solution phase, all the samples show nearly superimposable extinction spectra, besides a slight broadening upon increasing generation (Figure S6, $\lambda_{max} \approx 522$ nm), which indicate that the size and shape uniformity of the particles is preserved through the ligand exchange (Figure S7). When deposited onto thin films, the gold NPs show a redshift and broadening of the visible plasmon resonance compared to the isolated particles. The shift of the plasmon energy from the solution value is largest for Au@DDT and smallest for Au@G4, reflecting the differences in the interparticle spacing within those materials (Table 1).

Jain et al. demonstrated that the distance dependence of the absorption properties in pairs of noble metal nanoparticles (normalized to the isolated wavelength as $\Delta\lambda/\lambda_0$) obeys a universal scaling according to eq 1:

$$\Delta\lambda/\lambda_0 = ae^{-x/t} \quad (1)$$

where x is the reduced spacing, obtained by dividing the edge-to-edge separation (s, s', Table 1) with the diameter of the NP (ϕ = 5.8 nm), and both the parameters a and t depending on the interparticle environment and resonator material, respectively.[11] This equation was empirically verified using lithographically fabricated nanodisk pairs and data from solution-phase measurements of DNA-coupled Au NPs with variable DNA base pair spacings.[58] For Au NP pairs, the value of t has been found to range between 0.18 and 0.27 and the value of a between 0.16 and 0.29.[11,58] Fitting our data on interparticle separation and plasmon shift to eq 1 provides an estimate of t = 0.30−0.31 and a = 0.36−0.39 (Figure S8 for s and s', respectively), similar to the universal scaling which has been found in previous studies albeit with slightly higher values for both parameters. However, these results were obtained with smaller particles, much smaller absolute spacings than those obtained from DNA-based systems,[58] and confirmed in three-dimensional solids rather than small clusters.

Although TEM, SAXS, and UV (Figures 2 and 3) demonstrate control over the average spacing in the solid state for nanoparticles, under these experiments the samples do not demonstrate spontaneous long-range ordering. In Figure 4, we show self-assembled superlattices of Au NPs formed by slow evaporation of concentrated hexanes dispersions (5 mg mL^{-1}) of NPs on diethylene glycol. We first investigated superlattices of Au NPs with different generations of dendron coating. In Figure 4a, a self-assembled superlattice film of Au@DDT showing regions containing monolayer, bilayer, and trilayer is displayed. Large area superlattices, shown for Au@G1 and Au@G2 hybrids in Figure 4b,c can be obtained for NPs with dendritic ligands. These solids have much lower inorganic density than the Au@DDT superlattices, demonstrated in Figure 4c, which shows a bilayer region of Au@G2. At high magnification, such as the Au@G4 superlattice shown in Figure 4d, the dramatically larger interparticle distances (~12 nm) in the superlattice with dendron ligands become obvious.

DOI: 10.1021/jacs.5b06306
J. Am. Chem. Soc. 2015, 137, 10728−10734

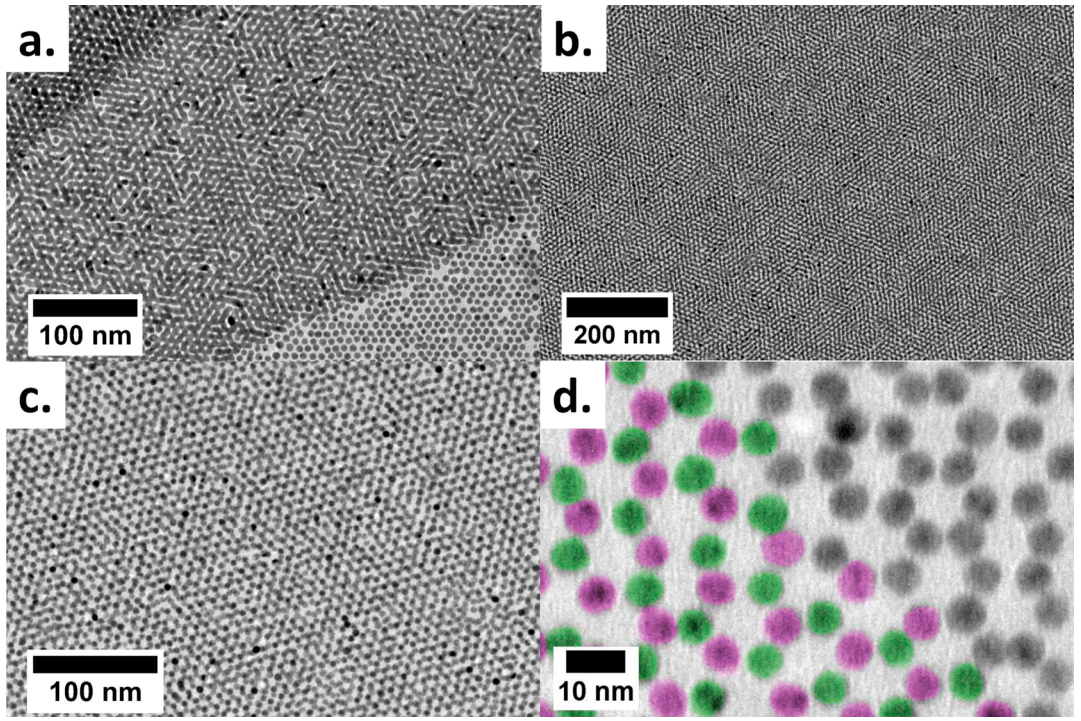

Figure 4. TEM micrographs of (a) Au@DDT forming monolayer, bilayer, and trilayer in an *hcp* superlattice film. (b) Multilayer superlattice film of Au@G1 hybrid. (c) Bilayer superlattice film of Au@G2. (d) High magnification of Au@G4 superlattice bilayer with partial coloration of the A and B layers in green and purple, evidencing theoretically expected moiré patterns. Average interparticular distances, d_{TEM}(nm) = 8.3 (Au@DDT), 10.1 (Au@G1), 11.3 (Au@G2), 12.5 (Au@G4).

Typically, in all cases, the Au NP superlattices form close-packed *hcp* assemblies; small regions of *fcc* arrangements (i.e., ABC stacks) were nevertheless sparingly found over very small areas (Figure S9). Although these hybrids have a "soft" corona, the formation of close-packed superlattices as shown in Figure 4 is still consistent with a model of entropy-driven crystallization of hard spheres, as the Au@L hybrids are *a priori* spherical building blocks that occupy the highest possible volume fraction. Because the contribution of the ligand shell to the volume of the building block increases with the generation of ligand, the inorganic density of the close-packed superlattices decreases (see also Figure S5).[59]

The dendron-based strategy outlined above allows access to more complex self-assembled structures of a single inorganic building block by combing the Au@L hybrids with different effective diameters (i.e., with different generation coatings): two superlattice structures of the AB_{13} and AB_5 types,[60] respectively, which are only otherwise known in binary compounds, are reported in Figure 5. For instance, when the monodisperse Au@DDT and Au@G2 hybrids are mixed, the effective diameter of the individual building blocks is adjusted to obtain a solid phase isostructural with the binary compound $NaZn_{13}$ (Figure 5a).[61] Mixing Au@G1 and Au@G4 hybrids, which have closer relative diameters, yields regions of a phase isostructural with $CaCu_5$ (Figure 5b). Both of these crystal structures are known in binary elemental and colloidal systems, but they are not formed in other single-component assemblies (Figure S10).

The first-order effect driving self-assembly into these binary superlattices is still the result of the coassembly of differently sized, monodisperse spheres. Although the starting point to explain the formation of these structures also relies on close packing for spheres with different diameters, but this is not necessarily sufficient to explain the observed assemblies because they do not represent the highest possible packing fractions at the size ratios estimated in from Table 1 (Figure S10). In the $NaZn_{13}$ structure, the Au@G2 hybrids, with an effective diameter (ϕ_{hyb}, Table 1) of 10.8 nm act as the larger spheres forming a simple cubic sublattice. Au@DDT hybrids, with an effective diameter of 8.2 nm form slightly distorted icosohedra in the interstices of the simple cubic lattice. Slight polydispersity is known to increase the space-filling of this structure, but at the diameter ratio of the Au@L samples used here ($\gamma \approx 0.76$), $NaZn_{13}$ structures show space filling of 59%, substantially less than single-component materials and other possible quasi-binary structures.[62,63] Indeed, $NaZn_{13}$ structures were observed to coexist with single-component superlattices of Au@DDT particles (Figure S12). To obtain the observed $CaCu_5$ structure, Au@G4 hybrids, with an effective diameter of 12.2 nm, act as the larger spheres, and Au@G1 hybrids, with an effective diameter of 10.2 nm, act as the smaller spheres. Again, space filling is an incomplete explanation for the observed $CaCu_5$ phase, which is less dense (62% at the size ratio of 0.84% used here) than single-component assemblies or other potential quasi-binary structures (e.g., CuAu).

The failure of simple hard sphere models may be explained by the fact that ligand-coated NPs are, on close inspection, neither hard nor spherical. Recent work by Boles and Talapin[64] suggests that "softness", or the relative volume of the organic shell of hydrophobic NPs, alters and enhances coassembly compared to hard systems by increasing the total filling fraction beyond that which is expected from a hard-sphere model. This has been used to explain, for example, the observation of both *fcc* and *bcc* single-component structures, although we did not observe *bcc* structures in any of the Au@L hybrids. Large organic volume fractions, as in this work, allow deformation of the spherical coronae of particles into Voronoï polyhedra that

DOI: 10.1021/jacs.5b06306
J. Am. Chem. Soc. 2015, 137, 10728−10734

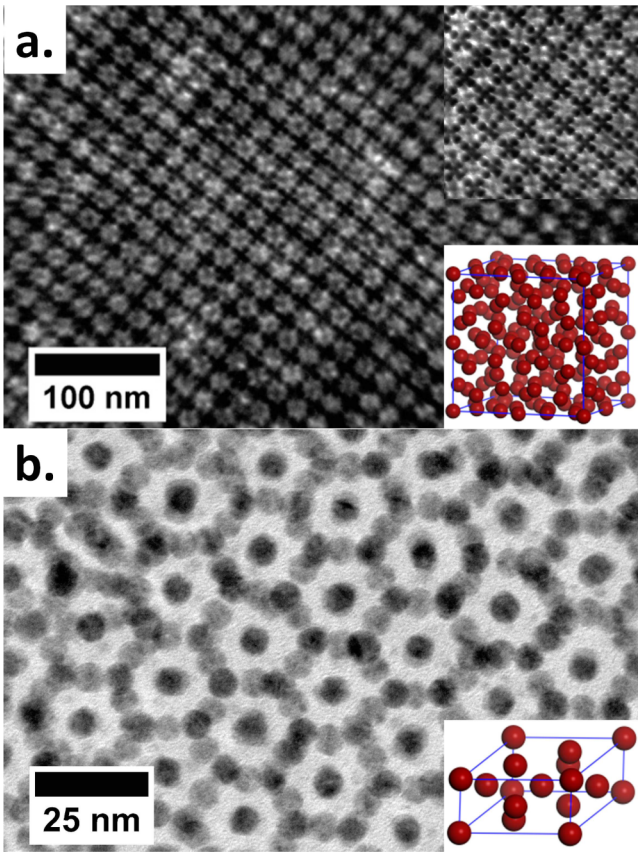

Figure 5. (a) TEM micrograph of [100] zone axis of a cubic $NaZn_{13}$ superlattice (Figure S11) comprised of Au@DDT and Au@G2 blends. Inset upper right is a thinner region of the sample. Inset lower right is a diagram of the unit cell [A_8B_{104}: $a \approx 38.7 \pm 0.7$ nm (TEM)], which contains 112 Au NPs. (b) TEM micrograph of [001] zone axis of a $CaCu_5$ superlattice (Figure S11) formed from a mixture of Au@G1 and Au@G4 hybrids. Inset lower right is a drawing of the unit cell [AB_5: $a \approx 20.7$ nm (TEM)], which contains six Au NPs.

allow maximum space filling. In addition, Boles and Talapin[64] observed that the preferred coordination number decreases with increases in the softness of the ligand shell. These two phenomena explain the formation of nominally poorer space-filling $NaZn_{13}$ and $CaCu_5$ structures made of soft Au@L hybrids, as opposed to the more dense quasi-binary phases or phase-separated single-component structures.

CONCLUSIONS

We have demonstrated that lipophilic, highly flexible dendritic ligands of several generations tethered to the surface of gold NPs can control their spacing and their assemblies in the solid state. By changing the dendritic generation grafted on the particle surface, we systematically were able to tune the interparticle distances between Au NPs over a range intermediate between that of DNA-stabilized particles and spacings available with commercial reagents, therefore providing an additional tool to engineer interparticle spacing in films and nanocomposites. Last, despite the relative simplicity of the ligand structure, the differentiation of the Au NP species with different dendritic tethers was used to generate unprecedented complex single-component NP superlattices, and opens new frontiers in the field of NPs assemblies. Indeed, this important last result is very promising and motivates the exploration of many other binary combinations of dendronized nanoparticulate hybrids, considering various dendritic structures and peripheral groups, and expanding the range of inorganic cores to different chemical compositions, sizes and shapes, to fabricate more exotic and functional multicomponent superlattices, i.e., metamaterials with modulable and enhanced properties.

ASSOCIATED CONTENT

Supporting Information

The Supporting Information is available free of charge on the ACS Publications website at DOI: 10.1021/jacs.5b06306.

Full characterization of organic compounds, additional microscopy, supporting spectroscopy (PDF)

AUTHOR INFORMATION

Corresponding Authors

*bdonnio@ipcms.unistra.fr

*cbmurray@sas.upenn.edu

Present Address

⊥Department of Chemical Engineering and SUNCAT Center for Interface Science and Catalysis, Stanford University, Stanford, CA 94305 (USA).

Notes

The authors declare the following competing financial interest(s): A provisional patent on this work has been filed under the number RD 2015/009-US-PSP.

ACKNOWLEDGMENTS

B.D. and D.J. thank the CNRS, UPENN and Solvay through the COMPASS Lab in partnership with the Penn's NSF MRSEC under Award No. DMR-112090. B.D. acknowledges additional support from the ANR Programme blanc, META-BIP, 12BS10-003. Part of this work was supported by the Office of Naval Research MURI award No. ONR-N00014-10-1-0942. D.R.K. acknowledges the Roy and Diana Vagelos Scholars Program in the Molecular Life Sciences. C.B.M. acknowledges the Richard Perry University Professorship.

REFERENCES

(1) Redl, F. X.; Cho, K.-S.; Murray, C. B.; O'Brien, S. *Nature* **2003**, *423*, 968−971.
(2) Shevchenko, E. V.; Talapin, D. V.; Kotov, N. A.; O'Brien, S.; Murray, C. B. *Nature* **2006**, *439*, 55−59.
(3) Xu, L.; Ma, W.; Wang, L.; Xu, C.; Kuang, H.; Kotov, N. A. *Chem. Soc. Rev.* **2013**, *42*, 3114−3126.
(4) Nie, Z.; Petukhova, A.; Kumacheva, E. *Nat. Nanotechnol.* **2010**, *5*, 15−25.
(5) Dong, A.; Chen, J.; Vora, P. M.; Kikkawa, J. M.; Murray, C. B. *Nature* **2010**, *466*, 474−477.
(6) Talapin, D. V.; Lee, J.-S.; Kovalenko, M. V.; Shevchenko, E. V. *Chem. Rev.* **2010**, *110*, 389−458.
(7) Kovalenko, M. V.; Manna, L.; Cabot, A.; Hens, Z.; Talapin, D. V.; Kagan, C. R.; Klimov, V. I.; Rogach, A. L.; Reiss, P.; Milliron, D. J.; Guyot-Sionnnest, P.; Konstantatos, G.; Parak, W. J.; Hyeon, T.; Korgel, B. A.; Murray, C. B.; Heiss, W. *ACS Nano* **2015**, *9*, 1012−1057.
(8) Sönnichsen, C.; Reinhard, B. M.; Liphardt, J.; Alivisatos, A. P. *Nat. Biotechnol.* **2005**, *23*, 741−745.
(9) Storhoff, J. J.; Lazarides, A. A.; Mucic, R. C.; Mirkin, C. A.; Letsinger, R. L.; Schatz, G. C. *J. Am. Chem. Soc.* **2000**, *122*, 4640−4650.
(10) Su, K. H.; Wei, Q. H.; Zhang, X.; Mock, J. J.; Smith, D. R.; Schultz, S. *Nano Lett.* **2003**, *3*, 1087−1090.

DOI: 10.1021/jacs.5b06306
J. Am. Chem. Soc. 2015, 137, 10728−10734

(11) Jain, P. K.; Huang, W.; El-Sayed, M. A. *Nano Lett.* **2007**, *7*, 2080−2088.
(12) Myroshnychenko, V.; Rodríguez-Fernández, J.; Pastoriza-Santos, I.; Funston, A. M.; Novo, C.; Mulvaney, P.; Liz-Marzán, L. M.; García de Abajo, F. J. *Chem. Soc. Rev.* **2008**, *37*, 1792−1805.
(13) Choi, J. Y.; Kim, Y. T.; Seo, T. S. *ACS Nano* **2013**, *7*, 2627−2633.
(14) Mirkin, C. A.; Letsinger, R. L.; Mucic, R. C.; Storhoff, J. J. *Nature* **1996**, *382*, 607−609.
(15) Elghanian, R.; Storhoff, J. J.; Mucic, R. C.; Letsinger, R. L.; Mirkin, C. A. *Science* **1997**, *277*, 1078−1081.
(16) Macfarlane, R. J.; Lee, B.; Jones, M. R.; Harris, N.; Schatz, G. C.; Mirkin, C. A. *Science* **2011**, *334*, 204−208.
(17) Sharma, J.; Chhabra, R.; Cheng, A.; Brownell, J.; Liu, Y.; Yan, H. *Science* **2009**, *323*, 112−116.
(18) Lau, K. L.; Hamblin, G. D.; Sleiman, H. F. *Small* **2014**, *10*, 660−666.
(19) Lan, X.; Chen, Z.; Liu, B. J.; Ren, B.; Henzie, J.; Wang, Q. *Small* **2013**, *9*, 2308−2315.
(20) Stamatoiu, O.; Mirzaei, J.; Feng, X.; Hegmann, T. *Top. Curr. Chem.* **2012**, *318*, 331−393.
(21) Nealon, G. L.; Greget, R.; Dominguez, C.; Nagy, Z. T.; Guillon, D.; Gallani, J.-L.; Donnio, B. *Beilstein J. Org. Chem.* **2012**, *8*, 349−370.
(22) Lewandowski, W.; Wójcik, M.; Górecka, E. *ChemPhysChem* **2014**, *15*, 1283−1295.
(23) Saliba, S.; Mingotaud, C.; Kahn, M. L.; Marty, J.-D. *Nanoscale* **2013**, *5*, 6641−6661.
(24) Blanc, C.; Coursault, D.; Lacaze, E. *Liq. Cryst. Rev.* **2013**, *1*, 83−109.
(25) Chiu, J. J.; Kim, B. J.; Kramer, E. J.; Pine, D. J. *J. Am. Chem. Soc.* **2005**, *127*, 5036−5037.
(26) Jones, M. R.; Osberg, K. D.; MacFarlane, R. J.; Langille, M. R.; Mirkin, C. A. *Chem. Rev.* **2011**, *111*, 3736−3827.
(27) Wilner, O. I.; Willner, I. *Chem. Rev.* **2012**, *112*, 2528−2556.
(28) Srivastava, S.; Frankamp, B. L.; Rotello, V. M. *Chem. Mater.* **2005**, *17*, 487−490.
(29) Grayson, S. M.; Fréchet, J. M. J. *Chem. Rev.* **2001**, *101*, 3819−3868.
(30) Carlmark, A.; Hawker, C.; Hult, A.; Malkoch, M. *Chem. Soc. Rev.* **2009**, *38*, 352−362.
(31) Newkome, G. R.; Shreiner, C. *Chem. Rev.* **2010**, *110*, 6338−6442.
(32) Sowinska, M.; Urbanczyk-Lipkowska, Z. *New J. Chem.* **2014**, *38*, 2168−2203.
(33) Gopidas, K. R.; Whitesell, J. K.; Fox, M. A. *J. Am. Chem. Soc.* **2003**, *125*, 6491−6502.
(34) Bronstein, L. M.; Shifrina, Z. B. *Chem. Rev.* **2011**, *111*, 5301−5344.
(35) Daniel, M.-C.; Astruc, D. *Chem. Rev.* **2004**, *104*, 293−346.
(36) Shon, Y.-S.; Choi, D. *Curr. Nanosci.* **2007**, *3*, 245−254.
(37) Advincula, R. C. *Dalton Trans.* **2006**, 2778−2784.
(38) Fleutot, S.; Nealon, G. L.; Pauly, M.; Pichon, B. P.; Leuvrey, C.; Drillon, M.; Gallani, J.-L.; Guillon, D.; Donnio, B.; Begin-Colin, S. *Nanoscale* **2013**, *5*, 1507−1516.
(39) Donnio, B.; García-Vázquez, P.; Gallani, J. L.; Guillon, D.; Terazzi, E. *Adv. Mater.* **2007**, *19*, 3534−3539.
(40) Kanie, K.; Matsubara, M.; Zeng, X.; Liu, F.; Ungar, G.; Nakamura, H.; Muramatsu, A. *J. Am. Chem. Soc.* **2012**, *134*, 808−811.
(41) Mischler, S.; Guerra, S.; Deschenaux, R. *Chem. Commun.* **2012**, *48*, 2183−2185.
(42) Li, H.; Li, Z.; Wu, L.; Zhang, Y.; Yu, M.; Wei, L. *Langmuir* **2013**, *29*, 3943−3949.
(43) Brunetti, V.; Bouchet, L. M.; Strumia, M. C. *Nanoscale* **2015**, *7*, 3808−3816.
(44) Tekade, R. K.; Tekade, M.; Kumar, M.; Chauhan, A. S. *Pharm. Res.* **2015**, *32*, 910−928.
(45) Park, M.-H.; Kim, S. T.; Rana, S.; Solfiell, D.; Jeong, Y.; Duncan, B.; Yan, B.; Aksoy, B.; Rotello, V. M. *Nanoscale* **2013**, *5*, 7805−7808.
(46) Walter, A.; Garofalo, A.; Parat, A.; Jouhannaud, J.; Pourroy, G.; Voirin, E.; Laurent, S.; Bonazza, P.; Taleb, J.; Billotey, C.; Vander Elst, L.; Muller, R. N.; Begin-Colin, S.; Felder-Flesch, D. *J. Mater. Chem. B* **2015**, *3*, 1484−1494.
(47) Daniel, M.-C.; Ruiz, J.; Nlate, S.; Palumbo, J.; Blais, J.-C.; Astruc, D. *Chem. Commun.* **2001**, 2000−2001.
(48) Daniel, M.-C.; Ruiz, J.; Nlate, S.; Blais, J.-C.; Astruc, D. *J. Am. Chem. Soc.* **2003**, *125*, 2617−2628.
(49) Wang, D.; Deraedt, C.; Salmon, L.; Labrugère, C.; Etienne, L.; Ruiz, J.; Astruc, D. *Chem. - Eur. J.* **2015**, *21*, 1508−1519.
(50) Gonzàlez De Rivera, F.; Angurell, I.; Rossell, O.; Seco, M.; Llorca, J. *J. Organomet. Chem.* **2012**, *715*, 13−18.
(51) Ihre, H.; Hult, A.; Söderlind, E. *J. Am. Chem. Soc.* **1996**, *118*, 6388−6395.
(52) Ihre, H.; Padilla De Jesús, O. L.; Fréchet, J. M. J. *J. Am. Chem. Soc.* **2001**, *123*, 5908−5917.
(53) Barnard, A.; Posocco, P.; Pricl, S.; Calderon, M.; Haag, R.; Hwang, M. E.; Shum, V. W. T.; Pack, D. W.; Smith, D. K. *J. Am. Chem. Soc.* **2011**, *133*, 20288−20300.
(54) Kowalczyk, W.; Mascaraque, A.; Sánchez-Navarro, M.; Rojo, J.; Andreu, D. *Eur. J. Org. Chem.* **2012**, *2012*, 4565−4573.
(55) Cho, T. J.; Zangmeister, R. A.; MacCuspie, R. I.; Patri, A. K.; Hackley, V. A. *Chem. Mater.* **2011**, *23*, 2665−2676.
(56) Hostetler, M. J.; Wingate, J. E.; Zhong, C.-J.; Harris, J. E.; Vachet, R. W.; Clark, M. R.; Londono, J. D.; Green, S. J.; Stokes, J. J.; Wignall, G. D.; Glish, G. L.; Porter, M. D.; Evans, N. D.; Murray, R. W. *Langmuir* **1998**, *14*, 17−30.
(57) Marcos, M.; Giménez, R.; Serrano, J. L.; Donnio, B.; Heinrich, B.; Guillon, D. *Chem. - Eur. J.* **2001**, *7*, 1006−1013.
(58) Reinhard, B. M.; Siu, M.; Agarwal, H.; Alivisatos, A. P.; Liphardt. *Nano Lett.* **2005**, *5*, 2246−2252.
(59) Pusey, P. N.; van Megen, W. *Nature* **1986**, *320*, 340−342.
(60) Chen, Z.; Moore, J.; Radtke, G.; Sirringhaus, H.; O'Brien, S. *J. Am. Chem. Soc.* **2007**, *129*, 15702−15709.
(61) Shevchenko, E. V.; Talapin, D. V.; O'brien, S.; Murray, C. B. *J. Am. Chem. Soc.* **2005**, *127*, 8741−8747.
(62) Murray, M. J.; Sanders, J. V. *Philos. Mag. A* **1980**, *42*, 721−740.
(63) Podsiadlo, P.; Krylova, G. V.; Demortière, A.; Shevchenko, E. V. *J. Nanopart. Res.* **2011**, *13*, 15−32.
(64) Boles, M. A.; Talapin, D. V. *J. Am. Chem. Soc.* **2015**, *137*, 4494−4502.

DOI: 10.1021/jacs.5b06306
J. Am. Chem. Soc. 2015, 137, 10728−10734